Size dependence of microprobe dynamics during gelation of a discotic colloidal clay

Jason P. Rich

Department of Chemical Engineering, Massachusetts Institute of Technology, Cambridge, Massachusetts 02139

Gareth H. McKinley[a)]

Hatsopoulos Microfluids Laboratory, Massachusetts Institute of Technology, Cambridge, Massachusetts 02139

Patrick S. Doyle[a)]

Department of Chemical Engineering, Massachusetts Institute of Technology, Cambridge, Massachusetts 02139

(Received 25 August 2010; final revision received 7 December 2010; published 20 January 2011)

Synopsis

Soft materials, such as gels and colloidal glasses, often exhibit different rheological properties at bulk and microscopic scales as a result of their complex microstructure. This phenomenon has recently been demonstrated for a gel-forming aqueous dispersion of Laponite® clay [Oppong *et al.* Phys. Rev. E **78**, 021405 (2008)]. For this material, microrheology reveals a significantly weaker gel and a longer gelation time than bulk measurements. By performing multiple particle tracking microrheology experiments with different probe sizes, we show that length-scale–dependent rheology is a general feature of Laponite® gels. Small changes in probe size are accompanied by order of magnitude differences in the observed rheological properties and gelation time. The probe dynamics also exhibit size-dependent spatial heterogeneities that help to elucidate a microstructural length scale in the system. Through analytical theory and Brownian dynamics simulations, we find that the correlations described by previous authors between successive displacements of individual probes are more directly a result of material elasticity than of microstructural confinement. The apparent gelation times of dispersions with different Laponite® concentrations exhibit a self-similar dependence on probe size, suggesting a superposition of Laponite® concentration and probe size. From these observations, we propose an accordant description of the microstructural evolution of the gel. © *2011 The Society of Rheology.* [DOI: 10.1122/1.3532979]

I. INTRODUCTION

Colloidal gels are an important class of soft materials that are found throughout nature and used in many industrial applications. They typically consist of a suspension of col-

[a)]Authors to whom correspondence should be addressed; electronic addresses: gareth@mit.edu and pdoyle@mit.edu

loidal particles that undergoes dynamical arrest through the formation of an interconnected fractal-like network [Russel *et al.* (1989)]. This process, called gelation, can occur via equilibrium or non-equilibrium routes [Zaccarelli (2007)] and results in a soft viscoelastic solid called a gel state [Larson (1999)]. Though suspended particles are often spherical and uncharged, anisotropic charged particles like discotic colloidal clays are common in nature and are used as rheological modifiers in many applications, such as paints, drilling fluids, consumer products, and cosmetics [Grim (1968)]. Dispersions of discotic colloidal clays are attractive for applications because of their ability to form various types of arrested states with rich rheological behavior even at low clay concentrations (around 1 wt %) [Luckham and Rossi (1999)].

In this article, we investigate the gelation and rheological aging of aqueous dispersions of the synthetic clay Laponite RD® (Rockwood Additives, Gonzales, TX) by tracking the thermally driven motion of embedded microscopic probe particles [Gardel *et al.* (2005); Waigh (2005); Mason and Weitz (1995); Mason (2000)]. Individual Laponite® crystals consist of colloidal disklike particles about 30 nm in diameter and 1 nm in thickness, with a reduced molecular formula of $Na^{+}_{0.7}[Si_8Mg_{5.5}Li_{0.3}O_{20}(OH)_4]^{-}_{0.7}$ [van Olphen (1977)]. The disk geometry and size have been verified by small-angle x-ray scattering (SAXS) measurements [Mourchid *et al.* (1995a); Kroon *et al.* (1998)]. Due to the molecular structure of the Laponite® clay, platelets in aqueous dispersions exhibit a negative charge on each face and for pH less than about 11, appear to be positively charged along the rim [van Olphen (1977)]. Previous reports have indicated the necessity of the resulting face-to-rim attractions for inducing aggregation and gelation [Martin *et al.* (2002); Mongondry *et al.* (2004)]. Attractive and repulsive surface charge interactions can be tuned by adjusting the ionic strength I in the solution, which affects the extent of the electrical double layer [Russel *et al.* (1989)]. Therefore, ionic strength strongly influences the nature and kinetics of structural arrest as well as the dispersion mechanical properties [Mourchid *et al.* (1995a); Mourchid *et al.* (1995b); Tawari *et al.* (2001)].

When Laponite® is dispersed in water, the system evolves over time from a liquidlike state to a nonergodic disordered arrested state. During this process, known generally as *aging*, the mechanical properties of the material change over time as the microstructure develops. Aging in Laponite® dispersions has been studied by a number of authors using dynamic light scattering (DLS), in which the transition from a liquid to an arrested state is typically monitored by analyzing the growth over time of a non-ergodicity parameter [van Megen *et al.* (1991)]. Though the physical mechanism of the aging process and the nature of the nonergodic states that develop have been the subject of much debate, the current status of DLS studies of aging in Laponite® dispersions is well-summarized by Jabbari-Farouji *et al.* (2008b). Here the authors also present a state diagram obtained from DLS measurements that attempts to unify the long age time observations of previous studies. Different nonergodic states are identified that correspond to regions in the (ionic strength)–(Laponite® concentration) state diagram: gel, repulsive "Wigner" glass, and a so-called "attractive glass" or "cluster glass" [Shalkevich *et al.* (2007)]. Generally, high values of I result in the screening of repulsive charge interactions between platelets, leading to the dominance of attractive interactions and the emergence of a gel or attractive glass state for Laponite® concentrations greater than or equal to about 0.5 wt % [see also Ruzicka *et al.* (2006)]. For $I > 10$ mM, repulsive interactions are screened to the extent that bulk phase separation via flocculation occurs [Mourchid *et al.* (1995a); Ruzicka *et al.* (2006)]. At low I, long-range repulsive interactions dominate, leading to a repulsive colloidal glass, even for Laponite® concentrations as low as about 1 wt %. In this work, we use a relatively high ionic strength ($I = 5.9$ mM) and examine dispersions of low Laponite® concentration (~ 1 wt %). For this set of parameters, we expect that

attractive interactions will dominate, resulting in either a gel or an attractive glass state. Since an attractive glass shares many structural and mechanical features with a gel, including spatial heterogeneity [Jabbari-Farouji *et al.* (2008b)], we shall employ the terminology of gelation in our analysis. While we acknowledge that some of our samples might possibly be more accurately characterized as "attractive glasses" in the arrested state, the DLS observations of Jabbari-Farouji *et al.* (2008b) imply that such a distinction would have negligible effect on our results and analysis, and that the two states would be essentially indistinguishable from a microrheological perspective.

By combining small-angle x-ray and neutron scattering with static light scattering, Pignon *et al.* (1997) studied the physical structure of Laponite® dispersions in the gel state, obtaining the scattering curve over five orders of magnitude in length scale. Their results indicate that there are two scales of fractal organization. On length scales ranging from about a few clay platelets to about 1 μm, aggregates form that exhibit spatial variations in Laponite® density ("micro-domains" separated by "voids"). These aggregates are themselves loosely connected in a fractal network, with clusters of aggregates exhibiting sizes up to about 5 μm. Beyond this length scale, the dispersion appears homogeneous. Their observations also indicate that the characteristic sizes of aggregates and clusters, as well as their densities and fractal dimensions, are dependent on the Laponite® concentration and the ionic strength [Pignon *et al.* (1996)].

Motivated by applications of Laponite® and other colloidal clays as rheological modifiers, the aging process in Laponite® dispersions has also been studied using rheology experiments. This work has also been driven by the fact that Laponite® dispersions serve as model soft thixotropic materials. As the system ages and develops structure, the viscosity of the dispersion increases by orders of magnitude and a yield stress emerges, also increasing over time. Early work on Laponite® rheology was performed by Ramsay (1986) who observed that at long age times, both the storage modulus G' and the yield stress of the dispersion increase strongly with Laponite® concentration. At a given age time and Laponite® concentration, Mourchid *et al.* (1995b) observed that the linear viscoelastic moduli increase with ionic strength up to the point at which bulk phase separation occurs via flocculation. They also found that the bulk storage modulus G' is nearly independent of frequency at long age times, a result confirmed by Ewoldt *et al.* (2007), who explored the use of an aqueous Laponite® dispersion as a simulant for a mucin gel in robotic mechanical crawlers. In this article, the steady shear viscosity was reported to decrease sharply when the applied stress exceeds the yield stress. Cocard *et al.* (2000) studied the age time and frequency dependence of the linear viscoelastic moduli at low Laponite® concentration and moderate ionic strength, observing growth in both G' and G'' over time and an approximate power-law frequency dependence. These results are consistent with the formation of a self-similar network structure (i.e., a gel), and the gelation time t_{gel} is defined as the time at which the power-law exponents for the frequency dependence of G' and G'' are equal [Chambon and Winter (1987)]. Bonn *et al.* (2002a) attempted to fit the rheological behavior of Laponite® dispersions in the repulsive glass state to the "soft glassy rheology" (SGR) model [Sollich *et al.* (1997); Sollich *et al.* (1997); Fielding *et al.* (2000)]. Their findings indicate good agreement in the linear viscoelastic regime. The model also correctly predicts qualitative features of shear-thinning and shear rejuvenation, which refers to the reduction in relaxation time that occurs when shearing motion breaks apart the dispersion microstructure [Bonn *et al.* (2002b)]. The competition between aging and shear rejuvenation at a constant shear rate, a feature of the SGR model, was demonstrated in glass-forming Laponite® dispersions by Abou *et al.* (2003). Some deviations from the SGR model were observed at large strains, however, due to shear banding and a viscosity bifurcation, in which the viscosity grows

indefinitely at low applied shear stress but remains orders of magnitude lower when a critical shear stress is exceeded [Bonn *et al.* (2002a)]. The SGR model has recently been extended to capture these effects [Fielding *et al.* (2009)].

In the present paper, the method of multiple particle tracking (MPT) is used to study the rheological properties of aqueous Laponite® dispersions at the microscopic scale. As with most microrheology techniques, MPT relates the motion of embedded microscopic probe particles to the rheology of the surrounding fluid [MacKintosh and Schmidt (1999)]. In the case of MPT, probe motion is driven solely by Brownian bombardment, with many probes (~100) being simultaneously visualized via video fluorescence microscopy [Gardel *et al.* (2005)]. Due to the small Brownian stress acting on the probe particles (usually 0.01–1 Pa), and the limited spatial resolution of optical microscopes, MPT is best suited for fluids with moduli ≤ 1 Pa [Waigh (2005)]. Software has been developed by Crocker and Grier (1996) for extracting trajectories from movies of diffusing probe particles, allowing the calculation of the ensemble average mean-squared displacement as a function of lag time. This quantity can be related to the linear viscoelastic moduli $G'(\omega)$ and $G''(\omega)$ by a generalized Stokes–Einstein relation [Mason and Weitz (1995); Mason (2000); Squires and Mason (2010)]. If the probes are much larger than any characteristic microstructural length scale in the fluid, then microrheological results will match those on the bulk scale. If, however, there are microstructural length scales on the order of the probe size (as is the case in Laponite® dispersions for probes smaller than about 5 μm [Pignon *et al.* (1997)]), then the results will reflect the mechanical properties of the material on that length scale and will generally not match bulk measurements [Liu *et al.* (2006)]. Because individual probe trajectories are available, analysis is not limited to ensemble averages. In particular, significant insight can be gained into the local microenvironments of individual probe particles [Valentine *et al.* (2001)], although Levine and Lubensky (2001) showed using a two-fluid model that local dynamics cannot be completely decoupled from fluid properties farther from probes. A number of industrially and biologically relevant gel-forming materials have been studied recently with MPT including Carbopol gels [Oppong *et al.* (2006)], gellan gum [Caggioni *et al.* (2007)], oligopeptide dispersions [Savin and Doyle (2007a); Larsen and Furst (2008)], and hectorite clay dispersions [Houghton *et al.* (2008)].

Despite considerable interest in the bulk rheology and phase behavior of Laponite® dispersions, there have been relatively few studies of the rheology on the microscopic scale. Jabbari-Farouji *et al.* (2007) used an optical tweezer setup to validate the fluctuation-dissipation theorem in an aging Laponite® dispersion by comparing results from passive and active microrheology experiments. In a subsequent publication, the thermal fluctuations of embedded probe particles in an optical trap were monitored in both gel-forming and glass-forming dispersions [Jabbari-Farouji *et al.* (2008a)]. From a microrheological perspective, the aging behavior of the two types of dispersions was found to be similar, although an examination of particles at various positions revealed differences in the spatial distribution of probe dynamics. Dispersions in the glass state exhibited spatially homogeneous microrheology that matched bulk rheology measurements, while significant heterogeneity and discrepancies with bulk results were observed in the gel state. Using MPT, Oppong *et al.* (2008) performed a more detailed comparison of the rheology at bulk and microscopic scales during the gelation process, confirming the discrepancies and the spatial heterogeneities reported by Jabbari-Farouji *et al.* (2008a). Additionally, these authors found that as the system ages, probes exhibit correlations between successive displacements, which were reported to result from microstructural confinement.

The results of Oppong *et al.* (2008) imply that the local rheology and gelation prop-

erties of the dispersion, and therefore the nature of the probe dynamics, may generally depend on the length scale that is probed: that is, the rheology may be probe-size–dependent. DLS observations by Strachan *et al.* (2006) of probe-size–dependent diffusive behavior in the repulsive glass state support this notion. Measurements of the average diffusivity of various sized particles by Petit *et al.* (2009) using fluorescence recovery after photobleaching (FRAP) are also consistent with this hypothesis. FRAP results were interpreted in terms of a scale-dependent effective viscosity that increases with probe size.

In this paper, we use MPT to study the gelation of aqueous Laponite® dispersions at the microscopic scale, expanding on the comparisons of bulk and micro-scale rheology made by Oppong *et al.* (2008) to explore the probe-size dependence of the microrheology. Based on our observations at different length scales, we propose a description of the microstructural evolution with age time and check the consistency of this scenario with measurements of the heterogeneity of probe dynamics for various probe sizes. Further, by examining correlations between successive probe displacements, we find evidence of a microstructural length scale in the system, although we challenge the interpretation of correlations as necessarily a result of microstructural confinement. Motivated by the probe-size dependence of our microrheological observations, in Sec. III E, we propose a common scaling for the gelation time that collapses data at different Laponite® concentrations and probe sizes.

II. EXPERIMENT

A. Sample preparation

Laponite RD® powder was obtained from Rockwood Additives. To prepare the clay dispersion, dry Laponite® powder is added to an aqueous buffer of pH $\approx$ 10 consisting of 1.8 mM NaOH and 4.1 mM $NaHCO_3$. The purpose of the buffer is to avoid the dissolution of Laponite® platelets, which has been observed at lower pH [Thompson and Butterworth (1992)] and to fix the solvent ionic strength at I=5.9 mM. The dispersion is kept under N_2 gas in order to prevent the uptake of CO_2, which would lower the solution pH and contribute to the dissociation of platelets [Mourchid *et al.* (1995a); Mourchid and Levitz (1998); Martin *et al.* (2002)]. After mixing vigorously for at least 1.5 h, the clay dispersion is passed through a 0.8 μm filter, breaking apart most of the remaining aggregates with a strong shear [Bonn *et al.* (1999)]. This filtration marks the point of zero age time t_w, in accordance with previous work on Laponite® dispersions [Abou *et al.* (2001)], and structuring of the clay begins thereafter as the system ages. Petit *et al.* (2009) demonstrated that about 7% of the initial Laponite® concentration is lost when dispersions of about 3 wt % Laponite® are passed through 0.45 μm filters. However, since the present study uses filters with larger pores (0.8 μm) and dispersions of lower concentration (presumably reducing the size of aggregates), it is assumed that filtration does not change the nominal concentration of Laponite®.

B. Multiple particle tracking

Immediately following filtering, fluorescent microparticles [Fluoresbrite® Yellow Green (YG) Carboxylate Microspheres from Polysciences, Inc.] are added to a concentration of about $\phi \sim 0.01$ vol % or about 100 particles per microscope view frame depending on the particle size. The fluorescent particle concentration is chosen to achieve a large number of individual particle trajectories with approximately non-interacting particles. After vortex mixing for about 15 s, the fluorescent particles are randomly dispersed

in the sample. The additional rejuvenation of the sample due to vortex mixing is minimal since it is conducted immediately after filtering.

It is important to consider the electrostatic and van der Waals interactions between probes and Laponite® particles, which could affect microrheological measurements [Valentine *et al.* (2004)]. Fluoresbrite® YG Carboxylate Microspheres were shown to be negatively charged in aqueous solutions close to the pH used in the present work, with a zeta potential of about −40 mV [Wegmann *et al.* (2008)]. Additionally, Laponite® particles exhibit surface charges of about $-700e$ per particle in aqueous solution, where e is the elementary charge [Martin *et al.* (2002)]. In order to determine the significance of probe–clay colloidal interactions, solution microcalorimetry measurements were performed using an Isothermal Titration Calorimeter (Nano ITC from TA Instruments) [O'Brien *et al.* (2000)]. When titrating a probe dispersion of 0.004 vol % (probe radius $a=0.161$ μm) into 0.04 vol % Laponite®, the probe-clay interaction energy was found to be about 35 mJ/g of Laponite®: less than the Laponite® dilution enthalpy into buffer at the same concentration (200 mJ/g of Laponite®) and below the reliable resolution of the instrument. This result implies that such interactions can be safely neglected.

After incorporating the probe particles, the dispersion is sealed in a sample chamber consisting of two cover slips separated by 250 μm thick spacers and mounted on a microscope (Carl Zeiss Optical, Axiovert 40 CFL). Experiments are performed at room temperature, $T \approx 23 \pm 0.5$ °C. A 63× water-immersion objective (N.A.=1.2) is used for all particle sizes except the largest particles, with radius $a=1.040$ μm, for which a 20× objective (N.A.=0.5) is used. An HBO 100 Mercury lamp (Carl Zeiss Optical), with an HBO 103 bulb (Osram) and an XF130-2 filter set (Omega Optical), is used to excite the particles and isolate their fluorescent emission. Movies of particle dynamics are captured with a charge coupled device (CCD) camera (Hitachi KP-M1A) having a variable shutter speed between 1/60 s and 1/10 000 s set to frame integration mode. SCION IMAGE software is used to record movies at a rate of 30 frames/s over the span of 1 min. Each video frame consists of two interlaced fields (the odd or even rows of the CCD matrix) that are exposed 1/60 s apart, requiring each frame to be de-interlaced during the movie analysis. The interlacing also results in a loss of resolution in the spatial direction perpendicular to the interlacing [Crocker and Grier (1996)]; thus, particle displacements in this study are only analyzed in the horizontal direction (the x-direction). Movies of probe particle diffusion are analyzed to obtain particle trajectories using publically available software developed by Crocker and Grier (1996).[1] Typical probe particle trajectories in 1 wt % Laponite® at various dispersion age times are shown in Fig. 1(a), from which the decreased mobility of the particles with age is immediately apparent. The most fundamental quantitative result extracted from probe trajectories is the mean-squared displacement (MSD) $\langle \Delta x^2(\tau) \rangle = \langle x(t+\tau) - x(t) \rangle$ as a function of the lag time τ. If the MSD data are smoothly varying, it can generally be fitted to a local power law [Mason (2000)],

$$\langle \Delta x^2(\tau) \rangle = 2D\tau^{\alpha(\tau)} \tag{1}$$

Here D is the probe diffusivity and $\alpha(\tau)$ is the diffusive exponent, equivalent to the logarithmic slope of the mean-squared displacement:

[1]http://www.physics.emory.edu/~weeks/idl/, "Particle Tracking Using IDL," site maintained by Eric Weeks.

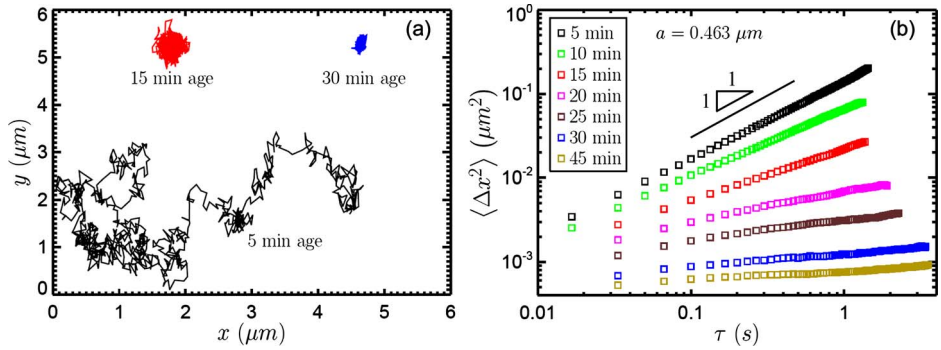

FIG. 1. (a) Typical trajectories of fluorescent probe particles with radius $a=0.463$ μm in 1 wt % Laponite® at various age times. Though particles exhibit diffusive motion at early age times, trajectories become increasingly localized as the dispersion ages. At late age times, probe particles fluctuate around a fixed central position. (b) The most fundamental quantitative result of multiple particle tracking is the mean-squared displacement $\langle \Delta x^2(\tau) \rangle$ as a function of lag time τ, shown here for various age times of a 1 wt % Laponite® dispersion and a probe radius of $a=0.463$ μm. At early age times, the probe motion is approximately diffusive and the logarithmic slope is close to 1. As the dispersion ages, the logarithmic slope decreases, and a plateau that is characteristic of a gel is eventually apparent at long lag times.

$$\alpha(\tau) = \frac{d \ln \langle \Delta x^2 \rangle}{d \ln \tau} \tag{2}$$

$\alpha(\tau)=1$ for diffusion in a Newtonian fluid, whereas probes in non-Newtonian fluids generally exhibit sub-diffusion with $0<\alpha(\tau)<1$. Unbiased statistical results for the ensemble average of MSD and the ensemble variance of MSD as a function of lag time τ are calculated using the estimators described by Savin and Doyle (2007b) for multiple particle tracking in heterogeneous systems. Software to implement these calculations in the IDL language is publically available.[2] Measured MSD data are corrected for static error by subtracting the apparent MSD of probe particles immobilized in a 3 wt % agarose gel [Savin and Doyle (2005b)]. Typical results for the MSD as a function of τ and dispersion age time t_w are shown in Fig. 1(b). As expected for a system that gels over time, the data exhibit a logarithmic slope $\alpha(\tau)$ close to 1 at early age times, with the slope decreasing as the material ages. After gelation, the MSD exhibits a plateau at long lag times.

Measurements of $\langle \Delta x^2(\tau) \rangle$ can be used to obtain the linear viscoelastic moduli via a generalized Stokes–Einstein relation [Mason and Weitz (1995); Squires and Mason (2010)]. This relation assumes that the probe particle inertia is negligible and that the probes experience a homogeneous continuum local environment. For smoothly varying MSD data capable of being fitted to the form in Eq. (1), the generalized Stokes–Einstein relation simplifies to the expression [Mason (2000)],

$$G^*(\omega = 1/\tau) = \left\{ \frac{1}{a \langle \Delta x^2(\tau) \rangle} \right\} \frac{k_B T}{3\pi} \frac{\exp[i\pi\alpha(\tau)/2]}{\Gamma[1+\alpha(\tau)]} \tag{3}$$

Here $G^*(\omega)=G'(\omega)+iG''(\omega)$ is the complex modulus, a is the probe radius, k_B is the Boltzmann constant, and T is the temperature. Γ represents the Γ-function. The angular frequency ω is the inverse of the lag time τ that is probed.

[2]http://web.mit.edu/savin/Public/.Tutorial/ "Microrheology of Heterogeneous Systems"© T. Savin.

C. Bulk rheology

Bulk rheology measurements are made using an ARG-2 stress-controlled rheometer from TA Instruments. In order to obtain reliable data in the pre-gel state at early age times when the viscosity of the Laponite® dispersion is quite low, an aluminum double-gap concentric cylinder Couette geometry is used, maximizing solid-liquid contact. The inner stator of the geometry has a radius of 20.00 mm, and the inner and outer rotor radii are 20.38 and 21.96 mm, respectively. The fluid sits in two gaps on either side of the rotor, both having a thickness of 0.38 mm, with an immersed cylindrical height of 59.5 mm. The Couette cell is equipped with water circulation tubes for temperature control and is maintained at the same temperature as microrheology experiments at $T=23\pm0.1\ ^{\circ}\mathrm{C}$. The Laponite® dispersion is prepared in the same way as in the microrheology experiments and is introduced into the Couette cell immediately after filtering, which we again mark as the time of zero age. Subsequently, the sample is pre-sheared at a shear rate of $\dot{\gamma}=250\ \mathrm{s}^{-1}$ for 30 s prior to measurement, helping to ensure a reproducible initial condition. Though the pre-shear may keep aggregates from forming and partially rejuvenate the fluid [Bonn *et al.* (2002a)], we find this additional rejuvenating effect to be negligible when the pre-shear is performed immediately after filtration. Oscillatory time sweep tests are used to measure the linear viscoelastic moduli, G' and G'', as a function of age time at a constant angular frequency of $\omega=1\ \mathrm{rad/s}$. In order to obtain reliable measurements at early age times, an oscillatory stress of amplitude $\sigma_0=0.02\ \mathrm{Pa}$ is initially applied, with this first step terminating once the strain amplitude γ_0 decreases to $\gamma_0=0.02$. Though strains in this step may initially appear to be in the nonlinear regime, the material is still essentially a viscous liquid, so that results are approximately strain independent. Once the strain amplitude decreases to $\gamma_0=0.02$, a second step applies a continuous oscillatory strain with a constant amplitude of $\gamma_0=0.02$. We have checked that the rheometer feedback mechanism is sufficient to maintain the applied strain within 0.02 ± 0.001.

III. RESULTS AND DISCUSSION

A. Probe-size effects on rheology

It was previously noted that the diffusive exponent $\alpha(\tau)$ in Eq. (1) describes the nature of the probe diffusion in the fluid (i.e., Newtonian diffusion or sub-diffusion). For a continuum fluid with homogeneous rheological properties across the length scales being probed, $\alpha(\tau)$ is purely a fluid property and thus should be independent of probe size. Therefore, we see from Eq. (3) that if the material exhibits the same properties at all length scales probed, the factor $a\langle\Delta x^2(\tau)\rangle$ will be independent of probe size. In Fig. 2, $a\langle\Delta x^2(\tau)\rangle$ is plotted as a function of lag time τ for four different probe sizes in an aging 1 wt % Laponite® dispersion. Though there is reasonably good agreement between different probe sizes at early age times, significant deviations are observed as the material ages. This is seen more clearly in Fig. 3, where the factor $a\langle\Delta x^2\rangle$ is plotted as a function of the age time t_w for the four probe sizes at a single value of the lag time, $\tau=0.3\ \mathrm{s}$. The data show that at 30 min age, for example, values of $a\langle\Delta x^2\rangle$ differ by more than an order of magnitude between the smallest and largest probes. These results indicate that there are strong probe-size effects and that the Laponite® dispersion is not a continuum fluid with homogeneous properties across the length scales probed.

Because of this scale-dependent behavior, it is necessary to proceed with care when extracting rheological properties from MPT measurements of $\langle\Delta x^2(\tau)\rangle$. We therefore consider rheological properties found from MPT as "effective" or "apparent" properties. The effective linear viscoelasticity at the microscopic scale can be calculated from the

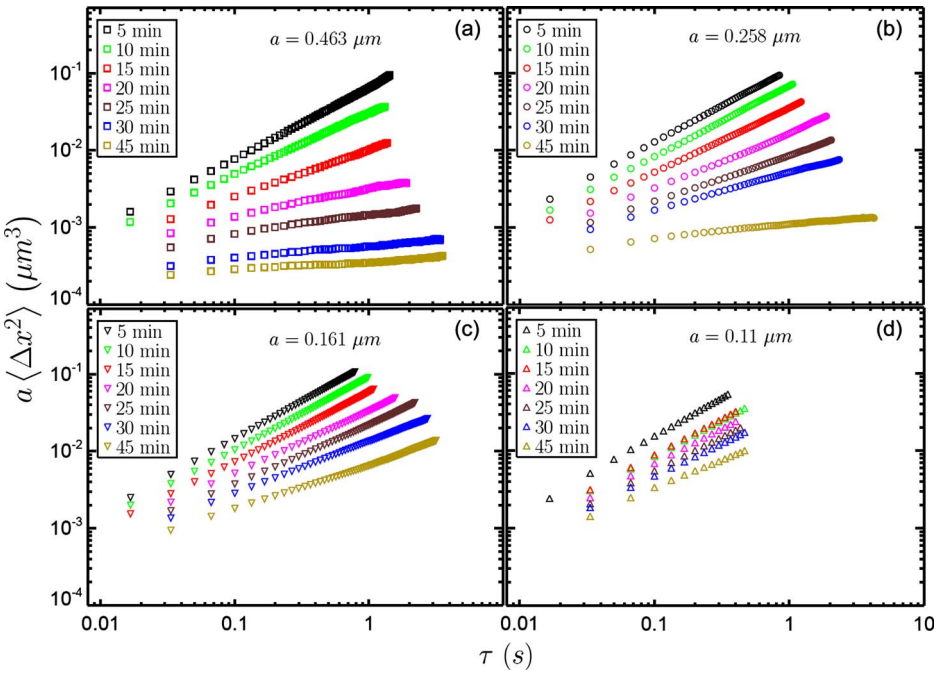

FIG. 2. Scaled MSD versus lag time for various probe sizes in an aging 1 wt % Laponite® dispersion. Probe radii are (a) a=0.463 μm, (b) a=0.258 μm, (c) a=0.161 μm, and (d) a=0.11 μm. For a homogeneous material with no length-scale dependence, data for all probe sizes should superimpose at a given dispersion age, in contrast to the results above. This non-superposition of data for various probe sizes implies that the dispersion structure and rheology are length-scale–dependent, and that the dispersion is heterogeneous in nature.

data in Fig. 2 by applying the generalized Stokes–Einstein relation in Eq. (3). When the diffusive exponent $\alpha(\tau)$ satisfies $0.5<\alpha(\tau)<1$, the material is dominated by viscous losses, whereas when $0<\alpha(\tau)<0.5$, the material is elastically dominated. Figure 4 shows the frequency dependence of the storage and loss moduli calculated from Eq. (3) at four age times for a representative probe size of a=0.463 μm. The loss modulus

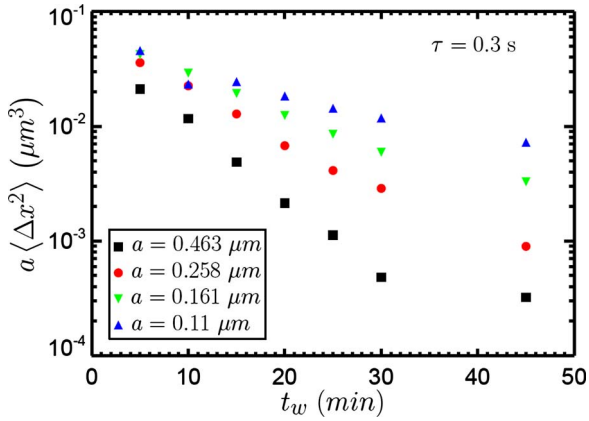

FIG. 3. Scaled MSD versus age time for various probe sizes in a 1 wt % Laponite® dispersion at a constant lag time of τ=0.3 s. Probe-size effects are clearly observed, as the non-superposition of data for different probe sizes indicates a variation in structure and rheology at different length scales. The deviations generally grow with age, signifying that the length-scale dependence of the rheology becomes more pronounced as the microstructure of the dispersion evolves.

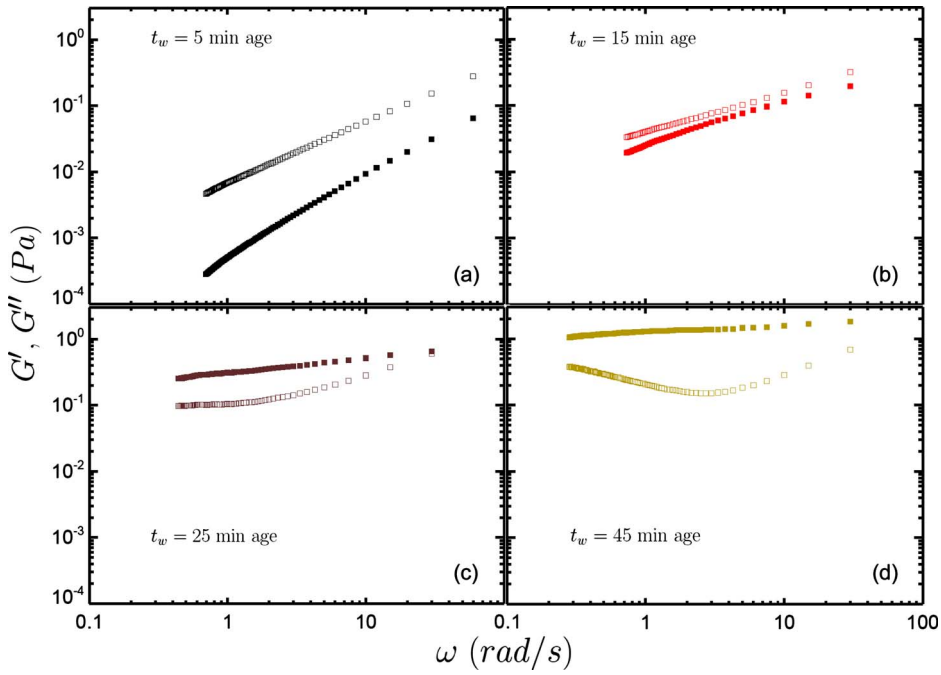

FIG. 4. Effective viscoelastic moduli calculated from microrheology versus angular frequency for 1 wt % Laponite® and a representative probe size of $a = 0.463$ μm at age times of (a) 5 min, (b) 15 min, (c) 25 min, and (d) 45 min. Filled symbols=G'; open symbols=G''. Though the dispersion is originally viscous-dominated, a crossover to elastic-dominated behavior occurs between 15 and 25 min of age. Near this crossover time at 15 min, the moduli have approximately the same frequency dependence, indicative of gelation [Chambon and Winter (1987)].

$G''(\omega)$ is dominant at early age times, indicating an initially viscous "sol." Both moduli increase with age time as the material develops structure and forms a gel, with the storage modulus $G'(\omega)$ eventually surpassing $G''(\omega)$. At late age times, $G'(\omega)$ is dominant and only weakly frequency-dependent, while $G''(\omega)$ exhibits a minimum value.

These results are consistent with a system undergoing gelation and are in qualitative agreement with previous observations on both bulk and microscopic scales [Cocard *et al.* (2000); Jabbari-Farouji *et al.* (2008a); Oppong *et al.* (2008)]. We note in Fig. 4(b) that at the time when $G'(\omega) \approx G''(\omega)$, both moduli exhibit approximately the same power-law frequency dependence. This is a hallmark of the critical gel point [Chambon and Winter (1987)], and indicates that the gelation time t_{gel} can be approximated as the time when the storage and loss moduli are equal. This is seen also in Fig. 5, where the loss tangent $\tan(\delta) = G''/G'$ is plotted as a function of angular frequency ω for various dispersion age times. According to the gelation theory of Chambon and Winter (1987), $\tan(\delta)$ is independent of frequency at the critical gel point. Interpolating between the data in Fig. 5, $\tan(\delta)$ is approximately independent of frequency at an age time of about 17 min; at this time $\tan(\delta) = G''/G' \approx 1$ for all frequencies. This again indicates that the gel point for this system is determined by the time when $G' \approx G''$. Similar behavior was seen for all probe sizes and Laponite® concentrations, and so we subsequently take the gelation time t_{gel} as the age time when $G' \approx G''$.

Applying Eq. (3) to MSD data for different probe sizes allows the direct comparison

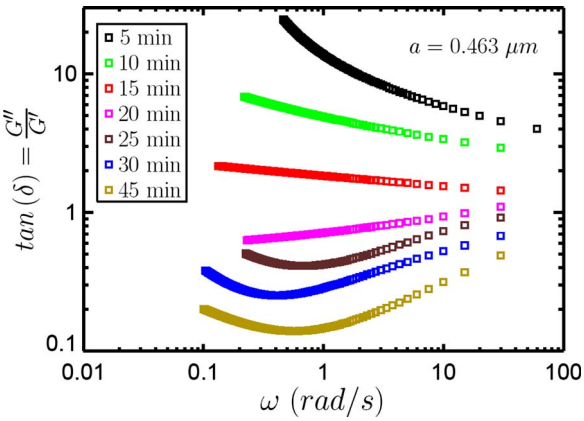

FIG. 5. Loss tangent calculated from microrheology versus angular frequency for 1 wt % Laponite® and a representative probe size of a=0.463 μm. tan(δ) is approximately independent of frequency when tan(δ) $=G''/G' \approx 1$, indicating that gelation occurs when $G' \approx G''$ [Chambon and Winter (1987)].

of apparent rheological properties in this heterogeneous clay dispersion at different length scales. Figure 6 shows the evolution of the storage and loss moduli with age time for a 1 wt % Laponite® dispersion at a representative frequency of ω=1 rad/s (i.e., lag time τ=1 s). Results for two different probe sizes are shown, as well as the bulk response. In agreement with Oppong *et al.* (2008), we observe significant deviation in the linear viscoelastic measurements between bulk and microscopic scales, with the bulk moduli exhibiting values that are at least an order of magnitude larger than those measured by MPT. The dispersion also reaches the gel point significantly earlier at the bulk scale. As the probe size is decreased from a=0.463 μm to a=0.11 μm, these trends continue. At a given age time, smaller probes result in lower measured viscoelastic moduli, sometimes by more than an order of magnitude. This indicates that the material is effectively a weaker gel at the smaller length scale. Additionally, t_{gel} is observed to be about 120 min

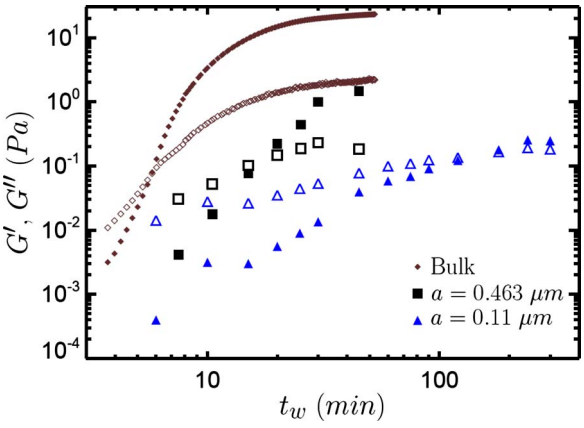

FIG. 6. Viscoelastic moduli as a function of age time for 1 wt % Laponite® at a representative frequency of ω=1 rad/s. Bulk rheology data as well as microrheology data for two different probe sizes are shown. G' =filled symbols; G''=open symbols. Though the trends are similar, at a given age time, probing at smaller length scales using microrheology results in lower apparent moduli (i.e., a weaker gel). The observed gelation time is also delayed when determined using a local versus a bulk measurement.

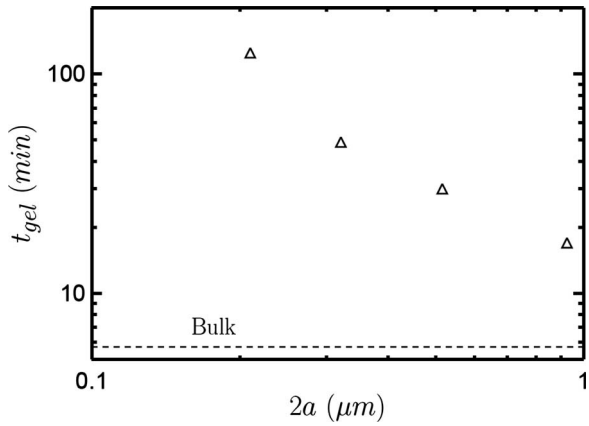

FIG. 7. Apparent gelation time versus probe diameter for a 1 wt % Laponite® dispersion. The bulk gelation time is denoted by the dashed line. From the bulk value to that observed for the smallest probe size, the gelation time changes by over an order of magnitude.

with the smaller probes, significantly delayed compared to the measurement of $t_{gel} = 17$ min with the larger probes. Specifically, at $t_{gel}(a = 0.463\ \mu\text{m}) = 17$ min, the smaller probes are still quite mobile, diffusing as if in a relatively low viscosity fluid with weak elasticity. The probe-size dependence of the apparent t_{gel} is shown in Fig. 7 for a 1 wt % Laponite® dispersion. Almost an order of magnitude increase in t_{gel} is observed as the probe diameter decreases by about an order of magnitude.

B. Microstructural description

We can conclude from these results that the Laponite® dispersion is not a continuum gel with homogeneous viscoelastic properties across the length scales probed; rather, in qualitative agreement with the long age time observations of Pignon *et al.* (1997), there must be microstructural features in the gel on length scales comparable to the probe particle sizes ($\sim 0.1-1\ \mu$m). This microstructure could result in different local environments, with different rheological properties, at different length scales. Since probe particle motions are directly related to structure and microrheological properties on the length scale of their size [Gardel *et al.* (2005)], this microstructure could provide an explanation for the observed phenomena. Because individual Laponite® particles are much smaller than the probes, the microstructure must result from larger aggregates of Laponite® particles, as proposed by Pignon *et al.* (1997). These aggregations can create gelled regions of relatively high Laponite® concentration, and regions where the Laponite® has been depleted, resulting in a type of porous network structure.

Based on our observations and those of previous authors, we propose the following scenario for the evolution of the microstructure with age time t_w. At early age times $t_w \ll t_{gel}$, the dispersion is homogeneous at the microscopic scale, with Laponite crystals (or small clusters of crystals) randomly distributed throughout the medium and diffusing freely. However, as the crystals diffuse, they encounter one another and occasionally aggregate due to van der Waals forces and electrostatic attraction. These aggregates grow more extended over time and eventually some span the container: this percolation characterizes the bulk gelation time. At this point, however, most of the dispersion still appears relatively homogeneous and viscous on the microscopic scale, and probe particles still diffuse through the sol with only slight hindrance [Oppong *et al.* (2008)]. As

the microstructure continues to develop, interconnected elastic clusters take up more and more of the dispersion volume, eventually trapping most of the larger probe particles in a viscoelastic gel network. Smaller probe particles, however, are not as restricted, and though some may have been trapped in gelled regions, most are still able to diffuse in non-gelled, or more weakly gelled pores in the aggregate structure. After a longer period of time, the smaller probes also become trapped by the shrinking pores in the gel network, leading eventually to the observation of a gelation time even at the length scale of the smallest probes.

If the proposed microstructural description is accurate, there are a number of indicators we would expect to observe. First, we would expect to see evidence of a spatially heterogeneous medium. That is, for intermediate t_w, probe particle trajectories should reflect the fact that some probes are trapped in more strongly gelled regions while others diffuse more freely in pores and weakly gelled regions. At a given t_w, we expect the microstructure will appear more or less heterogeneous at different length scales, so that the heterogeneity of the probe dynamics will also depend on the probe size. Second, we would expect probe trajectories to reflect the confinement due to the microstructure of the surrounding gel. Specifically, for particles diffusing in pores or other confined regions, we expect successive probe displacements over a sufficiently long lag time to be negatively correlated—having moved along a confined path over one time step, the probe will have a higher probability of rebounding in the opposite direction over the subsequent time step than a probe particle that is not confined, for which displacements would be uncorrelated [Doliwa and Heuer (1998); Weeks and Weitz (2002); Oppong *et al.* (2006); Oppong and de Bruyn (2007); Oppong *et al.* (2008)]. Lastly, analysis of these correlations and the spatial heterogeneity for different probe sizes should reveal a characteristic length scale (characteristic pore size, cluster size, etc.) for the microstructure at a given age time t_w.

C. Heterogeneity

Savin and Doyle (2007b) described a method for obtaining unbiased quantitative measures of spatial heterogeneity in a multiple particle tracking experiment.[3] Briefly, the result of the finite depth of tracking in MPT (i.e., the fact that particles diffuse in and out of focus in the z-direction) is that simple ensemble averaging of individual trajectory MSD's in a system with spatially heterogeneous rheology produces a statistical bias toward more mobile particles—these particles leave and enter the trackable depth more often, registering many short, mobile trajectories. If each trajectory is weighted by a factor proportional to its duration in time, however, unbiased estimators for the ensemble average of MSD and the ensemble variance of MSD can be calculated. From these estimators, a quantitative dimensionless measure of the spatial heterogeneity can be defined, which we shall call the heterogeneity ratio, HR:

$$HR = \frac{M_2(\tau)}{M_1(\tau)^2} \tag{4}$$

Here $M_1(\tau)$ is the estimator for the ensemble average of MSD, and $M_2(\tau)$ is the estimator for the ensemble variance of MSD, both functions of the lag time τ. As a point of reference, in a theoretical situation of MPT in an equally-weighted bimodal fluid where half the microscope view frame is water ($\eta_1 = 0.9$ mPa s), and half is a Newtonian fluid with viscosity $\eta_2 = 10\eta_1$, the result is a heterogeneity ratio of $HR \approx 0.6$. Additionally,

[3]Additional info available at http://web.mit.edu/savin/Public/.Tutorial/.

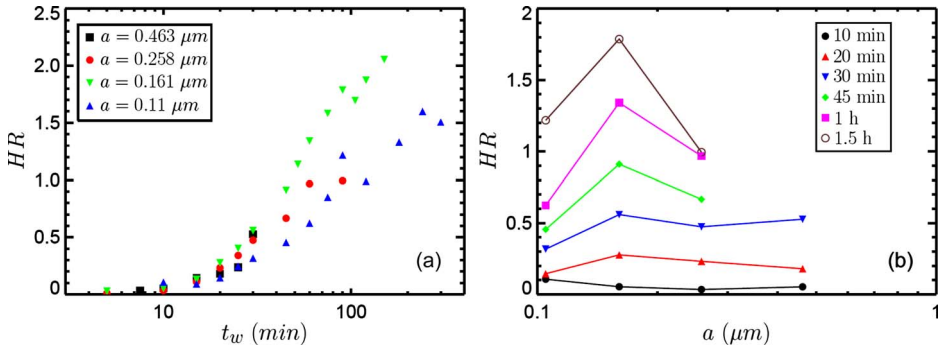

FIG. 8. Heterogeneity ratio *HR* for four probe sizes in 1 wt % Laponite® at a lag time of τ=0.33 s. (a) At early age times, heterogeneity is negligible for all probe sizes. As the dispersion ages and structure develops, significant heterogeneity is observed and *HR* becomes dependent on probe size. (b) At long age times, the relationship between *HR* and probe size is non-monotonic, with the heterogeneity exhibiting a maximum for a probe size of a=0.161 μm for $t_w \geq 30$ min.

exploratory calculations show that the maximum value of *HR* for an equally weighted bimodal Newtonian fluid is 3.

In Fig. 8(a), the heterogeneity ratio *HR* is plotted as a function of t_w for a 1 wt % Laponite® dispersion and four probe sizes at a lag time of τ=0.33 s. The Laponite® dispersion does exhibit significant heterogeneity and *HR* generally increases with t_w, consistent with our hypothesis for the microstructural evolution. Further, there is a non-monotonic dependence of *HR* on the probe size. This is highlighted in Fig. 8(b) where *HR* is plotted as a function of probe radius. For $t_w \geq 30$ min, *HR* is peaked at the intermediate probe size of a=0.161 μm. To understand why this occurs, we examine the particle trajectories in further detail to elucidate the nature of the heterogeneous probe dynamics.

Representative probe particle trajectories are shown in Fig. 9 for a 1 wt % Laponite® dispersion at t_w=90 min. Twenty discrete trajectories are shown for probes with radii (a)

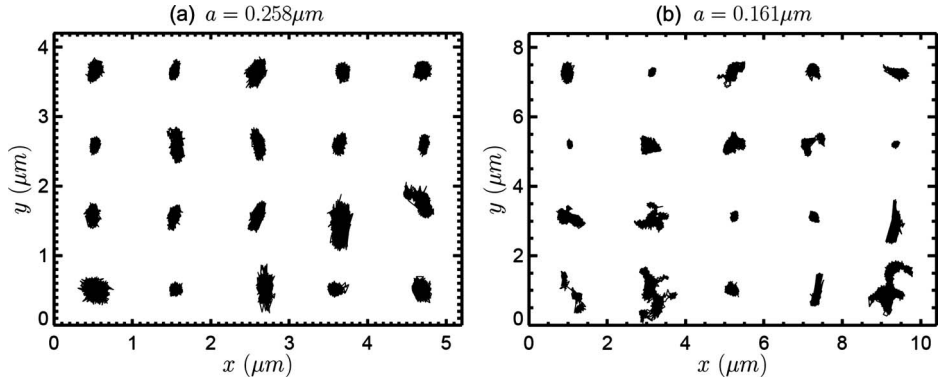

FIG. 9. Representative probe particle trajectories in 1 wt % Laponite® at t_w=90 min. Probe sizes are (a) a =0.258 μm and (b) a=0.161 μm, resulting in heterogeneity ratios of *HR*=0.99 and *HR*=1.78, respectively. While all the larger probes seem to diffuse around fixed locations, a significant fraction of the smaller probe trajectories exhibit more tortuous paths and/or "hopping" between distinct regions. At the same time, some of the smaller probe particles are relatively immobilized. The greater degree of variation in the dynamics for the smaller probe particles leads to the larger value of *HR*.

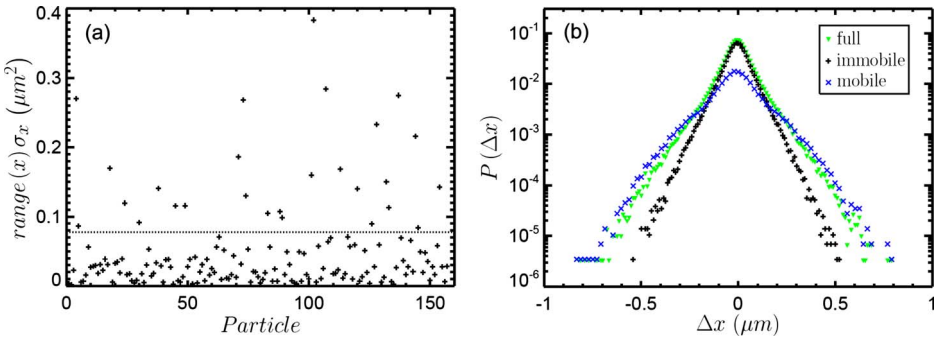

FIG. 10. Partitioning probe particles into two populations, mobile and immobile, for $a=0.161$ μm in 1 wt % Laponite® at $t_w=90$ min. (a) As an indicator of the mobility of particles, the product of the range and standard deviation of the x-coordinate position of probe particles is plotted. Particles falling above the dotted line are designated as a mobile population, and those below the line as an immobile population. (b) van Hove correlation data for mobile and immobile populations, as well as the full data set including all trajectories. Displacements over a lag time of $\tau=0.33$ s are shown. There is good agreement between the immobile population and the full data set for small displacements, while the mobile population characterizes the outer regions of large displacements.

$a=0.258$ μm and (b) $a=0.161$ μm, which exhibit heterogeneity ratios of $HR=0.99$ and $HR=1.72$, respectively. All of the larger probe particles seem to be immobilized to varying degrees, diffusing around fixed locations. In contrast, some of the 0.161 μm radius particles are immobilized, while others exhibit tortuous paths, as if exploring pores in the dispersion microstructure or "hopping" between adjacent distinct regions. As an approximation, it is possible to group these two types of trajectories into two populations, mobile and immobile, corresponding to spatial regions of two different average rheological properties. This is demonstrated in Fig. 10(a), where for each trajectory we plot the product of the range $[\max(r_x)-\min(r_x)]$ and the standard deviation σ_x of the x-coordinate position of the particle. The ordinate is therefore a simple measure of the mobility of a particle in a trajectory. Identifying an approximate cutoff, we designate the mobile particles as those falling above the dotted line, and the immobile particles as those falling below the dotted line. In Fig. 10(b), the probability distribution of displacements $P(\Delta x)$ over a lag time τ, known as the van Hove correlation function, is plotted for the mobile and immobile populations, as well as for the full data set with all trajectories. Displacements are taken over a lag time of $\tau=0.33$ s. The immobile population is in good agreement with the full data set for small displacements, while the mobile population characterizes the region of large displacements. This demonstrates that the majority of small displacements come from immobile particles, while mobile particles contribute most of the large displacements.

In Fig. 11, van Hove correlation data are shown for three different probe sizes in a 1 wt % Laponite® dispersion at an age time of $t_w=90$ min. Probe particle displacements are again taken over a lag time of $\tau=0.33$ s. If the material was homogeneous, the van Hove correlation function would exhibit a characteristic single Gaussian shape; deviations from single Gaussian behavior indicate heterogeneous probe dynamics. We note also that the heterogeneity ratio HR is similar to the non-Gaussian parameter N reported by previous authors [Oppong *et al.* (2008); Weeks *et al.* (2000); Kegel and van Blaaderen (2000)] except that statistical biases introduced by the finite depth of tracking in MPT are corrected. As expected based on the values of HR shown in Fig. 8 and the heterogeneous dynamics seen in Fig. 9, deviations from single Gaussian behavior are observed, with

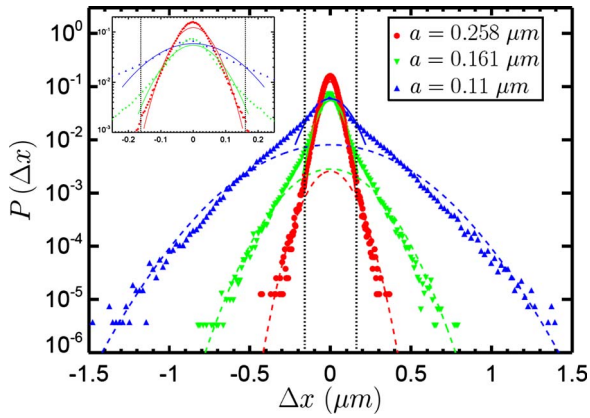

FIG. 11. van Hove correlation plots for three probe sizes in 1 wt % Laponite® at t_w=90 min. Displacements over a lag time of τ=0.33 s are shown. The distribution broadens as the probe radius decreases, reflecting the increased mobility of smaller particles. Deviations from single Gaussian behavior are a result of the spatial heterogeneity in the dispersion, with heterogeneity ratios of HR=0.99, 1.78, and 1.2 being observed for the probe sizes a=0.258 μm, 0.161 μm, and 0.11 μm, respectively. For each probe size, the data are sub-divided into two regions, each fitted by a Gaussian distribution. The fits to the immobile subsets with small displacements are shown as solid lines (with a zoom shown in the inset), and the fits to the subsets of mobile particles with large displacements are shown as dashed lines. The vertical black dotted lines correspond to $|\Delta x|$ =0.161 μm, which is equal to the intermediate probe size exhibiting a peak in heterogeneity in Fig. 8(b). The experimental data for all probe sizes begin to deviate from single Gaussian behavior very close to this value of $|\Delta x|$, suggesting that it may correspond to a characteristic microstructural length scale.

probes of radius a=0.161 μm exhibiting the most significant deviations. Motivated by the results from Fig. 10(b), each of the van Hove correlation functions are fitted with two Gaussian distributions [Kegel and van Blaaderen (2000)]: one capturing the small displacements (contributed mostly by immobile particles) and one capturing the large displacements (contributed mostly by mobile particles). The cutoff $|\Delta x|$ between these two regions identifies a characteristic length scale in the system. Probe particle displacements begin to deviate from single Gaussian behavior very close to $|\Delta x|$=0.161 μm, which is the value of the probe radius at which a peak in HR is observed. This value of $|\Delta x|$ =0.161 μm is denoted by the black dotted lines in Fig. 11. The fact that this cutoff $|\Delta x|$ is independent of probe size suggests that it is a microstructural length scale. We assert, therefore, that the peak in HR at a=0.161 μm and $t_w \geq 30$ min is due to a microstructural length scale in the dispersion that is very close in size to this probe radius. A similar length scale was measured by Mourchid *et al.* (1995a) and Pignon *et al.* (1997) using various scattering techniques. The tortuous paths exhibited by trajectories in Fig. 9(b) imply that this length scale may correspond to a characteristic pore radius in the gelled dispersion.

D. Correlations between successive probe displacements

The study of correlations between successive particle displacements has been adopted from examinations of cage effects in colloidal glasses [Doliwa and Heuer (1998); Weeks and Weitz (2002)] and applied to multiple particle tracking experiments, in which correlations yield insight into the confinement of probe particles by the surrounding fluid microstructure [Oppong *et al.* (2006); Oppong and de Bruyn (2007); Oppong *et al.* (2008)]. Let $\mathbf{r}_{01}$ and $\mathbf{r}_{12}$ represent successive two-dimensional displacement vectors of a probe particle over a lag time τ. That is, between time t_0 and $t_1 = t_0 + \tau$, the probe's

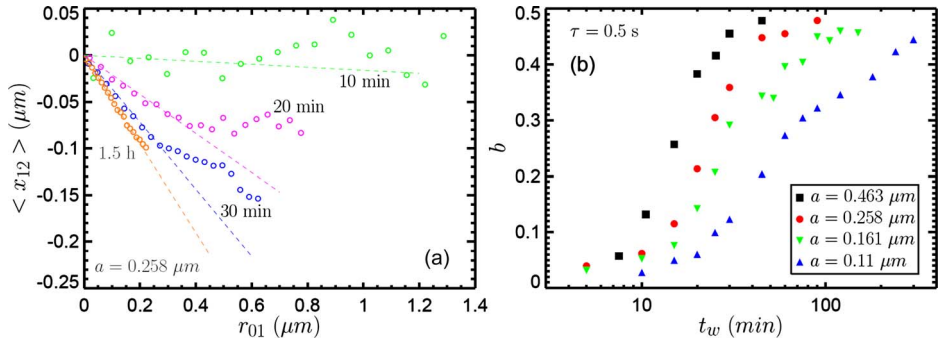

FIG. 12. (a) The degree of correlation between successive probe particle displacements at four age times in 1 wt % Laponite®. Data are shown for a representative probe size of $a=0.258$ μm and a lag time of $\tau=0.5$ s. Dashed lines show linear fits of the form $\langle x_{12}\rangle=-br_{01}$ to the first 10 points of data. The negative slope of the dashed lines gives the parameter b, which increases with the dispersion age time. The displacement magnitude r_{01} at which correlations deviate from linear behavior indicates a microstructural length scale in the system. (b) Evolution of the b parameter with age time for four probe sizes in 1 wt % Laponite®, over a lag time of $\tau=0.5$ s. The b parameter grows with age and exhibits probe-size dependence, though self-similar behavior is seen between all probe sizes. The data reach a plateau value of b slightly less than 0.5.

displacement in the plane of focus is given by $\mathbf{r}_{01}$, and between time t_1 and $t_2=t_1+\tau$, the probe's subsequent displacement is given by $\mathbf{r}_{12}$. If the probes are executing a random walk, as in a viscous Newtonian fluid, then $\mathbf{r}_{01}$ and $\mathbf{r}_{12}$ will be uncorrelated. Successive displacements will be correlated, however, if probes are confined by the fluid microstructure. The correlation between successive displacements $\langle x_{12}\rangle$ is defined as

$$\langle x_{12}\rangle=\left\langle\frac{\mathbf{r}_{01}\cdot\mathbf{r}_{12}}{r_{01}}\right\rangle \tag{5}$$

Here r_{01} is the magnitude of the initial displacement, $r_{01}=\|\mathbf{r}_{01}\|$, and angular brackets represent ensemble averages. To gain a better physical understanding of $\langle x_{12}\rangle$, consider a probe particle confined in a pore and assume its displacement over an initial lag time τ is $\mathbf{r}_{01}=\mathbf{r}(t_0+\tau)-\mathbf{r}(t_0)$. Therefore, $\mathbf{r}_{01}$ represents an accessible path for the confined probe, and in the subsequent time step τ there is an increased probability that the probe will retrace its steps through that known accessible path. In that case, $\mathbf{r}_{12}$ would be in the opposite direction of $\mathbf{r}_{01}$, so that $\mathbf{r}_{01}$ and $\mathbf{r}_{12}$ are negatively correlated. We therefore expect $\langle x_{12}\rangle$ to be negative when microstructural confinement affects probe motion.

$\langle x_{12}\rangle$ is plotted as a function of r_{01} in Fig. 12(a) at four age times for 1 wt % Laponite® and a representative probe size of $a=0.258$ μm. Correlations between successive displacements of duration $\tau=0.5$ s are shown. While values of $\langle x_{12}\rangle$ are scattered around 0 at $t_w=10$ min, the correlations grow in magnitude as the system ages. The degree of correlation also grows with the size of the initial displacement r_{01}, and we observe a linear relationship of the form $\langle x_{12}\rangle=-br_{01}$. The coefficient b, which grows with t_w as the microstructure develops, is reported to represent the ability of the fluid microstructure to restrict the motion of the probe particles [Oppong *et al.* (2008)]. b is plotted as a function of t_w for four probe sizes in Fig. 12(b). Though b is probe-size–dependent at a given t_w, data for different probe sizes exhibit self-similar age time dependence, suggesting a common scaling. At late age times, b seems to plateau at $b=0.5$ for all probe sizes. The fact that correlations become increasingly significant as the dispersion ages implies that microstructural confinement effects on probe motion are

important, which is consistent with our hypothesis for the microstructural evolution in Sec. III B.

In Fig. 12(a), the degree of correlation is seen to deviate from linear behavior past a critical value of r_{01} for $t_w > 10$ min. This value of r_{01} represents a microstructural length scale in the system. Though these results are in contrast to the results of Oppong *et al.* (2008), these authors use only a larger probe size ($a = 0.50$ μm), so that initial displacements r_{01} large enough to observe the deviation from linearity are inaccessible. Upon measuring this critical displacement $r_{01,crit}$ for various probe sizes and age times, we find $\bar{r}_{01,crit} \approx 0.33$ μm, approximately twice the length scale observed in Sec. III C from heterogeneity measurements. We propose that these two independent measurements actually reflect the same microstructural length scale, and that the difference by a factor of 2 is a result of the different methods of probing it.

Having examined the evolution of the b parameter and its probe-size dependence in an aging Laponite® dispersion, we now consider in more depth the physical meaning of b. It has been reported [Oppong *et al.* (2008)] that b reflects microstructural confinement; however, one could imagine that successive displacements may also be correlated for probes embedded in a model material with no microstructure but with viscoelasticity that persists on time scales of the lag time τ or longer. To investigate this, we consider probes suspended in a Kelvin–Voigt model viscoelastic solid, which is represented by a mechanical equivalent circuit of a spring and a dashpot in parallel. The linear spring has an elastic modulus G and the dashpot has a Newtonian viscosity η. The relaxation time of the material is therefore given by $\lambda_V = \eta/G$. The equation of motion for a Brownian probe particle diffusing in such a material is [Savin and Doyle (2005a)]

$$\lambda_V \lambda_I \ddot{\mathbf{r}}(t) + \lambda_V \dot{\mathbf{r}}(t) + \mathbf{r}(t) = \mathbf{f}(t)/6\pi aG \tag{6}$$

where $\lambda_I = m/6\pi aG\lambda_V$ is an inertial time scale (with m being the mass of the probe particle) and $\mathbf{f}(t)$ is the stochastic Brownian force [Volkov and Leonov (1996)]. By taking the Fourier transform of both sides of Eq. (6), we obtain an expression for the power spectral density of the position $S^*_{\mathbf{r}}(\omega) = \langle |\mathbf{r}^*|^2(\omega) \rangle$ [Savin and Doyle (2005a)],

$$S^*_{\mathbf{r}}(\omega) = \frac{\lambda_V k_B T/\pi aG}{(1 + \lambda_+^2 \omega^2)(1 + \lambda_-^2 \omega^2)} \tag{7}$$

where the roots $\lambda_\pm$ are given by

$$\lambda_\pm = \frac{\lambda_V}{2}(1 \pm \sqrt{1 - 4\lambda_I/\lambda_V}) \tag{8}$$

In writing Eq. (7), we have applied the fluctuation-dissipation theorem $S^*_{\mathbf{f}}(\omega) = \langle |\mathbf{f}^*|^2(\omega) \rangle = 36\pi aG\lambda_V k_B T$. Using the method detailed in Appendix A, we can obtain the relationship between $\langle x_{12} \rangle$ and r_{01},

$$\langle x_{12} \rangle = -\tfrac{1}{2}[1 - \exp(-\tau/\lambda_V)] r_{01} \tag{9}$$

where τ/λ_V is the ratio between the lag time and the material relaxation time. Comparing this expression to $\langle x_{12} \rangle = -b r_{01}$, we find a simple expression for b for probe particles embedded in a Kelvin–Voigt material,

$$b = \tfrac{1}{2}[1 - \exp(-\tau/\lambda_V)] \tag{10}$$

This expression is plotted in Fig. 13. In order to validate the approximations that were made to derive Eq. (10) (see Appendix A), we perform a Brownian dynamics (BD) simulation of a probe particle undergoing Brownian motion in a Kelvin–Voigt material.

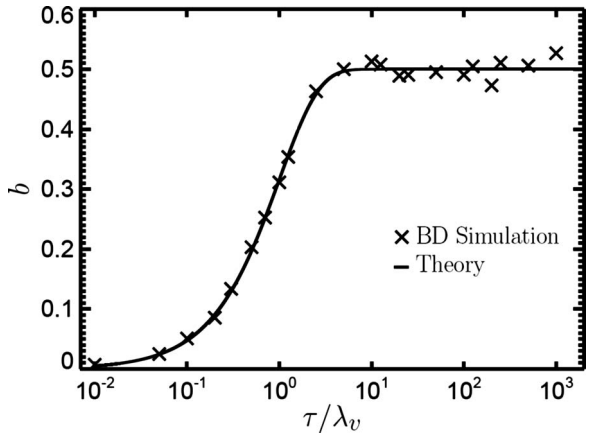

FIG. 13. The variation of b with the dimensionless lag time τ/λ_V for a Kelvin–Voigt material, from theory and BD simulation. Theoretical results match those from the BD simulation. The plot shows that nonzero values of b can result from elasticity even in a homogeneous material without microstructure. In the case of a Kelvin–Voigt material, b depends solely on the ratio of the relaxation time to the lag time that is probed.

The details of the simulation are given in Appendix B. Figure 13 shows that the simulation and the theoretical results match quantitatively. The fact that $b>0$ for the Kelvin–Voigt material demonstrates that if there is elasticity present, even a continuum material with no microstructural features can exhibit correlations between successive probe displacements. Furthermore, if the relaxation time λ_V is spatially homogeneous (i.e., independent of r_{01}), b is a constant at a given lag time τ, so that there is a linear relationship between $\langle x_{12}\rangle$ and r_{01} for all r_{01}. This indicates that the departure from linearity observed in Laponite® results from microstructural heterogeneities.

The connection between b and elasticity implies that the common scaling between the data for different probe sizes in Fig. 12(b) may be related to the development of elasticity in the material. That is, if b is plotted as a function of some measure of the local elasticity, the data for different probe sizes may collapse. With this motivation, we plot b as a function of the apparent storage modulus $G'(\omega)$ in Fig. 14, where ω is evaluated at the inverse of the correlation lag time $\omega=1/\tau$. The data for all probe sizes collapse onto a single curve. This suggests that b is more directly related to apparent elasticity than to microstructural confinement in Laponite® dispersions, though the observed elasticity is undoubtedly a result of the structural development in the material. The observation that $\langle x_{12}\rangle$ deviates from a linear variation with r_{01} beyond a critical displacement remains a strong indicator of a microstructural length scale.

E. Concentration effects

All of the experimental results presented thus far have been for a 1 wt % Laponite® dispersion. The observed probe size effects could be interpreted as indicating that at a given age time t_w, the dispersion "appears" more concentrated in Laponite® as the probe size increases. That is, at a given age time, smaller probes experience local environments that are on average like a relatively dilute dispersion, whereas larger probes experience local environments that are more characteristic of the bulk concentration. Recognizing this, we investigate the connection between probe size effects and Laponite® concentration. Specifically, we examine whether a superposition can be found between concentration and probe size.

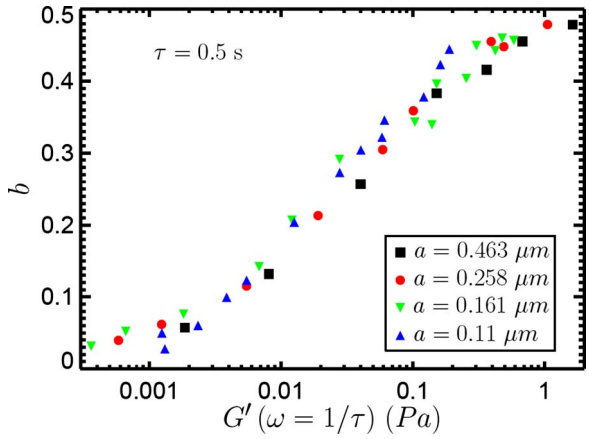

FIG. 14. b plotted against the measured storage modulus for various probe sizes in 1 wt % Laponite®, over a lag time of τ=0.5 s. $G'(\omega)$ is evaluated at a frequency of $\omega = 1/\tau = 2$ rad/s from MPT measurements at the corresponding probe size. The results for b from various probe sizes collapse, confirming the connection between b and the material elasticity and suggesting that b is more directly related to elasticity than to microstructural confinement for Laponite® dispersions.

Figure 15(a) shows the observed gelation time t_{gel} as a function of probe diameter for three different Laponite® concentrations. The gelation time t_{gel} exhibits a similar trend with probe size for all three dispersions, though the value of t_{gel} is highly sensitive to Laponite® concentration, decreasing rapidly as the concentration is increased by just 0.5 wt %.

We seek a relationship describing the scaling of t_{gel} with the probe radius a and the Laponite® concentration c, expressed in wt %. From Fig. 15(a), it appears that t_{gel} follows approximately a power-law scaling with probe size a for each concentration. Kroon *et al.* (1996) used dynamic light scattering to investigate the sol-gel transition of aqueous Laponite® dispersions with various concentrations. For dispersions with 2.2 wt % $\leq c \leq$ 3.4 wt % and no added salt, they found that the gelation time scales exponentially with

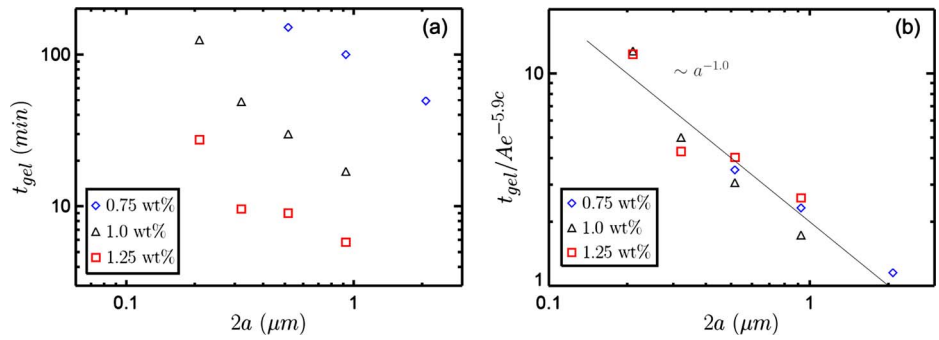

FIG. 15. (a) Apparent gelation time versus probe diameter for three Laponite® concentrations. The gelation time is very sensitive to the Laponite® concentration, decreasing rapidly for small increases in concentration. The probe-size dependence is similar for all three concentrations. (b) Gelation time data scaled by an exponential factor of the Laponite® concentration c in wt %. This scaling serves to collapse the gelation time data for the three concentrations examined onto a single curve, exhibiting a -1.0 power-law scaling with probe size. The existence of such a master curve is an indication of a concentration–probe-size superposition.

c according to $t_{gel} \sim \exp(-2.83c)$. Motivated by these observations, we therefore assume an empirical expression for t_{gel} of the form

$$t_{gel} = A a^{\beta} \exp(-\kappa c) \tag{11}$$

where A, β, and κ are constants determined by fitting this expression to the experimental data in Fig. 15(a). Using a nonlinear least-squares regression, we find the best-fit values to be $A=3613.7$, $\beta=-1.0$, and $\kappa=5.9$, for t_{gel} expressed in minutes and a expressed in micrometers. The fitted value of κ is indicative of the strong inverse relationship between gelation time and Laponite® concentration. That is, t_{gel} decreases rapidly even for slight increases in c. The discrepancy in the value of κ as compared to the result of Kroon *et al.* (1996) is likely due to the different experimental conditions and sample preparation procedure. In particular, in the present study we control the ionic strength I through the use of added salt, since it is known that the gelation dynamics are sensitive to I [Mourchid *et al.* (1995a); Mourchid *et al.* (1995b); Tawari *et al.* (2001)]. The nearly integer value of β suggests that there may be a relatively simple mechanism underlying the observed scaling, though we reserve a detailed mechanistic description for future communication. The ability of Eq. (11) to describe the experimental results is demonstrated in Fig. 15(b), where the gelation time data in Fig. 15(a) have been scaled by the exponential factor $A \exp(-5.9c)$. Data for the three different Laponite® concentrations collapse reasonably well onto a single curve with a scaling $\sim a^{-1.0}$, validating Eq. (11) and the values of the constants given above. The collapse also suggests a superposition between probe size and Laponite® concentration, with the product at_{gel} remaining essentially constant for a given Laponite® concentration over the range of probe sizes studied here.

IV. CONCLUSIONS

Many commercially and biologically relevant fluids exhibit different rheological properties at different length scales as a result of complex microstructure. In this communication, we have used multiple particle tracking microrheologies to explore how rheological properties vary with probe size in an aqueous dispersion of Laponite®, a discotic colloidal clay that forms an aging colloidal gel under appropriate conditions. We have shown that the microrheological properties are dependent on the probe particle size, implying that the dispersion is heterogeneous across different length scales. Probing at smaller length scales results in the observation of lower viscoelastic moduli and a delay in gelation time. We have also proposed a microstructural explanation for these phenomena: as the material ages, a porous network structure develops that traps larger probe particles, while smaller probes generally have more time to diffuse relatively unhindered through pores and more weakly gelled regions. In support of this hypothesis, we observed that the probe dynamics develop significant spatial heterogeneity as the system ages. Analysis of these heterogeneities for different probe sizes indicates a microstructural length scale in the system that is similar to the length scales measured previously by light scattering [Mourchid *et al.* (1995a); Pignon *et al.* (1997)]. In light of these results, it would be interesting to further investigate the microstructural heterogeneities and their associated length scales with two-point microrheology [Crocker *et al.* (2000)]. With this method, the viscoelastic moduli could be explored as a function of probe separation, although we reserve this study for future work. In addition to heterogeneities, we find that as the system ages the probe particles exhibit correlations between successive displacements, which has been reported to be evidence of microstructural confinement. However, by analyzing trajectories of a Brownian particle in a continuum Kelvin–Voigt material,

we find that correlations between successive probe displacements are more directly related to the apparent local elasticity. We propose that a better measure of the microstructual confinement is the length scale at which deviations from a simple linear scaling are observed in these successive correlations. An interesting problem for future work would be to determine the corresponding correlations for probes diffusing in a Newtonian fluid confined by solid walls, which provides a simple model of a porous microstructure. Finally, motivated by the observed probe-size dependence of rheological properties and the proposed microstructural description, we identify a concentration–probe-size superposition, obtaining approximate scalings for the observed gelation time as a function of probe size and Laponite® concentration.

The results presented in this article will aid in the understanding of the structure and rheology of aqueous Laponite® dispersions. Furthermore, the methods used here may also find broader general application to other structured complex fluids and gels. The methods are particularly suitable for analyzing materials that serve different functions at different length scales, and that as a result must have different rheological properties across length scales. Possible examples include the cell cytoskeleton, which provides structural stability on the length scale of the entire cell, but must also allow macromolecules and vesicles to diffuse within the pores. Finally, the results of this article show that multiple particle tracking can provide insight into the structure of evolving materials, even when the system is inhomogeneous at the probe length scale.

ACKNOWLEDGMENTS

Acknowledgment is made to the Donors of the American Chemical Society Petroleum Research Fund (ACS-PRF Grant No. 49956-ND9) for support of this research. J.P.R. acknowledges financial support from a National Defense Science and Engineering Graduate Fellowship (NDSEG) from the American Society of Engineering Education. The authors thank Matthew Helgeson for help with solution microcalorimetry experiments, and Thierry Savin and Daniel Trahan for useful discussions.

APPENDIX A: CORRELATIONS IN A KELVIN–VOIGT MATERIAL

To derive expressions for the correlations between successive displacements $\langle x_{12}\rangle$ and the b parameter for probe particles undergoing Brownian motion in a Kelvin–Voigt material, we begin with the autocorrelation function of the probe position $\mathbf{r}(t)$ over a lag time τ:

$$C_{\mathbf{r}}(\tau) = \langle \mathbf{r}(t+\tau)\cdot\mathbf{r}(t)\rangle - \langle \mathbf{r}(t)\rangle^2 \tag{A1}$$

Here brackets represent time averages. For successive probe displacements $\mathbf{r}_{01}$ and $\mathbf{r}_{12}$, each over a lag time τ, it can be shown that

$$\langle \mathbf{r}_{01}\cdot\mathbf{r}_{12}\rangle = 2C_{\mathbf{r}}(\tau) - C_{\mathbf{r}}(2\tau) - C_{\mathbf{r}}(0) \tag{A2}$$

$$\langle \mathbf{r}_{01}\cdot\mathbf{r}_{01}\rangle = 2C_{\mathbf{r}}(0) - 2C_{\mathbf{r}}(\tau) \tag{A3}$$

Here we have used the fact that $\langle \mathbf{r}(t)\rangle = 0$ in a Kelvin–Voigt material (i.e., the material is a viscoelastic solid). In order to proceed, we make the following approximations. First, we approximate $\langle \|\mathbf{r}_{01}\|\rangle = \langle \sqrt{\mathbf{r}_{01}\cdot\mathbf{r}_{01}}\rangle \approx \sqrt{\langle \mathbf{r}_{01}\cdot\mathbf{r}_{01}\rangle}$ where we have taken the square root outside of the average. Second, noting the form of $\langle x_{12}\rangle$ versus r_{01} in Eq. (5), we make the so-called "Peterlin approximation" that the average of a quotient is approximately equal to the quotient of the averages:

$$\langle x_{12}\rangle = \left\langle \frac{\mathbf{r}_{01}\cdot\mathbf{r}_{12}}{\|\mathbf{r}_{01}\|}\right\rangle = \left\langle \frac{\mathbf{r}_{01}\cdot\mathbf{r}_{12}}{\sqrt{\mathbf{r}_{01}\cdot\mathbf{r}_{01}}}\right\rangle \approx \frac{\langle \mathbf{r}_{01}\cdot\mathbf{r}_{12}\rangle}{\langle\sqrt{\mathbf{r}_{01}\cdot\mathbf{r}_{01}}\rangle} \approx \frac{\langle \mathbf{r}_{01}\cdot\mathbf{r}_{12}\rangle}{\sqrt{\langle \mathbf{r}_{01}\cdot\mathbf{r}_{01}\rangle}} \tag{A4}$$

Combining these approximations with Eq. (A2) and Eq. (A3) and using the fact that $r_{01}=\langle\|\mathbf{r}_{01}\|\rangle$, we arrive at an expression for $\langle x_{12}\rangle$ in terms of $C_{\mathbf{r}}(\tau)$ and r_{01}:

$$\langle x_{12}\rangle = \frac{2C_{\mathbf{r}}(\tau) - C_{\mathbf{r}}(2\tau) - C_{\mathbf{r}}(0)}{2C_{\mathbf{r}}(0) - 2C_{\mathbf{r}}(\tau)} r_{01} \tag{A5}$$

This expression shows a linear variation between $\langle x_{12}\rangle$ and r_{01} of the form $\langle x_{12}\rangle = -br_{01}$. The expression for b in terms of $C_{\mathbf{r}}(\tau)$ is therefore

$$b = -\frac{2C_{\mathbf{r}}(\tau) - C_{\mathbf{r}}(2\tau) - C_{\mathbf{r}}(0)}{2C_{\mathbf{r}}(0) - 2C_{\mathbf{r}}(\tau)} \tag{A6}$$

This expression can be simplified by recognizing that $C_{\mathbf{r}}(\tau)$ is the inverse Fourier transform of the power spectral density of the probe position $S^{*}_{\mathbf{r}}(\omega)$, given in Eq. (7) for Brownian probes embedded in a Kelvin–Voigt material:

$$C_{\mathbf{r}}(\tau) = \frac{(\lambda_+ + \lambda_-)k_BT}{4\pi aG}\left[\frac{e^{-\tau/\lambda_+} + e^{-\tau/\lambda_-}}{\lambda_+ + \lambda_-} + \frac{e^{-\tau/\lambda_+} - e^{-\tau/\lambda_-}}{\lambda_+ - \lambda_-}\right] \tag{A7}$$

where the roots $\lambda_{\pm}$ are given in Eq. (8). In realistic situations, the inertial time scale for the probe is many orders of magnitude less than the relaxation time of the material, so that $\lambda_I/\lambda_V \ll 1$. In this limit, $\lambda_+ \approx \lambda_V$ and $\lambda_- \approx 0$. Applying the inertia-less limit to Eq. (A7), we obtain

$$C_{\mathbf{r}}(\tau) = \frac{k_BT}{2\pi aG}\exp(-\tau/\lambda_V) \tag{A8}$$

The autocorrelation function of the probe position decays with a characteristic time constant λ_V. Finally, substituting this equation into Eq. (A6) yields a simple expression for b that matches Eq. (10):

$$b = \tfrac{1}{2}[1 - \exp(-\tau/\lambda_V)] \tag{A9}$$

$\langle x_{12}\rangle$ is then given by

$$\langle x_{12}\rangle = -\tfrac{1}{2}[1 - \exp(-\tau/\lambda_V)]r_{01} \tag{A10}$$

which matches Eq. (9). In the limit $\tau/\lambda_V \ll 1$, $b \to 0$, and there are no correlations between successive probe particle displacements. The lag time is not long enough for probe motions to be affected by the elasticity of the material. In the limit $\tau/\lambda_V \gg 1$, $b \to 0.5$, and the successive displacements of probe particles are significantly correlated. In this case, probe motions are highly influenced by the elasticity of the material over the time scale of the lag time τ.

Since a number of approximations were made to obtain these expressions, a BD simulation was conducted in order to check the theoretical results. The details of the simulation are given below in Appendix B.

APPENDIX B: BROWNIAN DYNAMICS SIMULATIONS IN A KELVIN–VOIGT MATERIAL

The equation of motion for a Brownian probe particle in a Kelvin–Voigt material is given in Eq. (6). We wish to solve this stochastic differential equation using BD. Physical

insight and computational efficiency can be gained by first using appropriate length and time scales to make the equation of motion dimensionless. We invoke the equipartition theorem for a tethered Brownian spring to obtain the scaling relationship,

$$GL^2 \sim \frac{k_B T}{a} \tag{B1}$$

where L is the characteristic length scale at which Brownian and elastic forces on the probe particle balance. Rearranging this expression and substituting $G=\eta/\lambda_V$ and $D=k_BT/6\pi\eta a$ give the length scale L to be

$$L=\sqrt{D\lambda_V} \tag{B2}$$

If we now take the characteristic time scale t^* to be the characteristic time for the probe to diffuse the distance L, we see from Eq. (B2) that $t^*=\lambda_V$. Applying this scaling, we obtain a dimensionless equation of motion:

$$\frac{\lambda_I}{\lambda_V}\ddot{\hat{\mathbf{r}}}(\hat{t})+\dot{\hat{\mathbf{r}}}(\hat{t})+\hat{\mathbf{r}}(\hat{t})=\frac{\mathbf{f}(\hat{t})}{6\pi aG}\sqrt{\frac{1}{\lambda_V D}} \tag{B3}$$

where $\hat{\mathbf{r}}(\hat{t})=\mathbf{r}(t)/L$ and over-dots represent derivatives with respect to the dimensionless time variable $\hat{t}=t/\lambda_V$. The right-hand side of Eq. (B3) is a dimensionless Brownian force $\hat{\mathbf{f}}(\hat{t})$:

$$\hat{\mathbf{f}}(\hat{t})=\frac{\mathbf{f}(t)}{6\pi aG}\sqrt{\frac{1}{\lambda_V D}}=\frac{\mathbf{f}(t)}{k_BT/L} \tag{B4}$$

This stochastic force is expressed at each dimensionless time step $\hat{t}=\hat{t}_n$ in terms of a random number $[r_n]$ taken from a uniform distribution with $[r_n]\in[-1/2,1/2]$.

$$\hat{\mathbf{f}}(\hat{t}_n)=\sqrt{\frac{24}{\Delta\hat{t}}}[r_n] \tag{B5}$$

Here $\Delta\hat{t}=\Delta t/\lambda_V$ is the dimensionless time increment. Substituting this expression into the right-hand side of Eq. (B3), we obtain a dimensionless equation of motion that can be solved numerically in Euler integration steps:

$$\frac{\lambda_I}{\lambda_V}\ddot{\hat{\mathbf{r}}}+\dot{\hat{\mathbf{r}}}+\hat{\mathbf{r}}=\sqrt{\frac{24}{\Delta\hat{t}}}[r_n] \tag{B6}$$

If we now take the inertialess limit $\lambda_I/\lambda_V \ll 1$, then the resulting equation of motion is

$$\dot{\hat{\mathbf{r}}}+\hat{\mathbf{r}}=\sqrt{\frac{24}{\Delta\hat{t}}}[r_n] \tag{B7}$$

There are no free parameters in this equation, indicating that the simulation needs only to be performed once in dimensionless coordinates in order to obtain a probe particle trajectory that can subsequently be analyzed for specific correlations. Therefore, correlations between successive displacements should only depend on the dimensionless lag time τ/λ_V. We run the simulation with a time step of $\Delta\hat{t}=0.001$ and a total of 5.0×10^8 time steps, exploring values of τ/λ_V from 10^{-2} to 10^3.

References

Abou, B., D. Bonn, and J. Meunier, "Aging dynamics in a colloidal glass," Phys. Rev. E **64**, 021510 (2001).

Abou, B., D. Bonn, and J. Meunier, "Nonlinear rheology of Laponite suspensions under an external drive," J. Rheol. **47**, 979–988 (2003).

Bonn, D., H. Kellay, H. Tanaka, G. Wegdam, and J. Meunier, "Laponite: What is the difference between a gel and a glass?," Langmuir **15**, 7534–7536 (1999).

Bonn, D., P. Coussot, H. T. Huynh, F. Bertrand, and G. Debrégeas, "Rheology of soft glassy materials," Europhys. Lett. **59**, 786–792 (2002a).

Bonn, D., S. Tanase, B. Abou, H. Tanaka, and J. Meunier, "Laponite: Aging and shear rejuvenation of a colloidal glass," Phys. Rev. Lett. **89**, 015701 (2002b).

Caggioni, M., P. T. Spicer, D. L. Blair, S. E. Lindberg, and D. A. Weitz, "Rheology and microrheology of a microstructured fluid: The gellan gum case," J. Rheol. **51**, 851–865 (2007).

Chambon, F., and H. H. Winter, "Linear viscoelasticity at the gel point of a cross-linking PDMS with imbalanced stoichiometry," J. Rheol. **31**, 683–697 (1987).

Cocard, S., J. F. Tassin, and T. Nicolai, "Dynamical mechanical properties of gelling colloidal disks," J. Rheol. **44**, 585–594 (2000).

Crocker, J. C., and D. G. Grier, "Methods of digital video microscopy for colloidal studies," J. Colloid Interface Sci. **179**, 298–310 (1996).

Crocker, J. C., M. T. Valentine, E. R. Weeks, T. Gisler, P. D. Kaplan, A. G. Yodh, and D. A. Weitz, "Two-point microrheology of inhomogeneous soft materials," Phys. Rev. Lett. **85**, 888–891 (2000).

Doliwa, B., and A. Heuer, "Cage effect, local anisotropies, and dynamic heterogeneities at the glass transition: A computer study of hard spheres," Phys. Rev. Lett. **80**, 4915–4918 (1998).

Ewoldt, R., C. Clasen, A. E. Hosoi, and G. H. McKinley, "Rheological fingerprinting of gastropod pedal mucus and synthetic complex fluids for biomimicking adhesive locomotion," Soft Matter **3**, 634–643 (2007).

Fielding, S. M., M. E. Cates, and P. Sollich, "Shear banding, aging and noise dynamics in soft glassy materials," Soft Matter **5**, 2378–2382 (2009).

Fielding, S. M., P. Solich, and M. E. Cates, "Aging and rheology in soft materials," J. Rheol. **44**, 323–369 (2000).

Gardel, M. L., M. T. Valentine, and D. A. Weitz, in *Microscale Diagnostic Techniques*, edited by K. S. Breuer (Springer, New York, 2005), Chap. 1.

Grim, R. E., *Clay Mineralogy* (McGraw-Hill, New York, 1968).

Houghton, H. A., I. A. Hasnain, and A. M. Donald, "Particle tracking to reveal gelation of hectorite dispersions," Eur. Phys. J. E **25**, 119–127 (2008).

Jabbari-Farouji, S., D. Mizuno, M. Atakhorrami, F. C. MacKintosh, C. F. Schmidt, E. Eiser, G. H. Wegdam, and D. Bonn, "Fluctuation-Dissipation Theorem in an aging colloidal glass," Phys. Rev. Lett. **98**, 108302 (2007).

Jabbari-Farouji, S., M. Atakhorram, D. Mizuno, E. Eiser, G. H. Wegdam, F. C. MacKintosh, D. Bonn, and C. F. Schmidt, "High-bandwidth viscoelastic properties of aging colloidal glasses and gels," Phys. Rev. E **78**, 061402 (2008a).

Jabbari-Farouji, S., H. Tanaka, G. H. Wegdam, and D. Bonn, "Multiple nonergodic disordered states in Laponite suspensions: A phase diagram," Phys. Rev. E **78**, 061405 (2008b).

Kegel, W. K., and A. van Blaaderen, "Direct observation of dynamical heterogeneities in colloidal hard-sphere suspensions," Science **287**, 290–293 (2000).

Kroon, M., W. L. Vos, and G. H. Wegdam, "Structure and formation of a gel of colloidal disks," Phys. Rev. E **57**, 1962–1972 (1998).

Kroon, M., G. H. Wegdam, and R. Sprik, "Dynamic light scattering studies on the sol-gel transition of a suspension of anisotropic colloidal particles," Phys. Rev. E **54**, 6541–6550 (1996).

Larsen, T. H., and E. M. Furst, "Microrheology of the liquid-solid transition during gelation," Phys. Rev. Lett. **100**, 146001 (2008).

Larson, R. G., *The Structure and Rheology of Complex Fluids* (Oxford University Press, New York, 1999).

Levine, A. J., and T. C. Lubensky, "Response function of a sphere in a viscoelastic two-fluid medium," Phys.

Rev. E **63**, 041510 (2001).

Liu, J., M. L. Gardel, K. Kroy, E. Frey, B. D. Hoffman, J. C. Crocker, A. R. Bausch, and D. A. Weitz, "Microrheology probes length scale dependent rheology," Phys. Rev. Lett. **96**, 118104 (2006).

Luckham, P. F., and S. Rossi, "The colloidal and rheological properties of bentonite suspensions," Adv. Colloid Interface Sci. **82**, 43–92 (1999).

MacKintosh, F. C., and C. F. Schmidt, "Microrheology," Curr. Opin. Colloid Interface Sci. **4**, 300–307 (1999).

Martin, C., F. Pignon, J.-M. Piau, A. Magnin, P. Lindner, and B. Cabane, "Dissociation of thixotropic clay gels," Phys. Rev. E **66**, 021401 (2002).

Mason, T. G., "Estimating the viscoelastic moduli of complex fluids using the Generalized Stokes–Einstein equation," Rheol. Acta **39**, 371–378 (2000).

Mason, T. G., and D. A. Weitz, "Optical measurements of frequency-dependent viscoelastic moduli of complex fluids," Phys. Rev. Lett. **74**, 1250–1253 (1995).

Mongondry, P., T. Nicolai, and J. F. Tassin, "Influence of pyrophosphate or polyethylene oxide on the aggregation and gelation of aqueous laponite dispersions," J. Colloid Interface Sci. **275**, 191–196 (2004).

Mourchid, A., A. Delville, J. Lambard, E. LeColier, and P. Levitz, "Phase diagram of colloidal dispersions of anisotropic charged particles: Equilibrium properties, structure, and rheology of Laponite suspensions," Langmuir **11**, 1942–1950 (1995a).

Mourchid, A., A. Delville, and P. Levitz, "Sol-gel transition of colloidal suspensions of anisotropic particles of laponite," Faraday Discuss. **101**, 275–285 (1995b).

Mourchid, A., and P. Levitz, "Long-term gelation of Laponite dispersions," Phys. Rev. E **57**, R4887–R4890 (1998).

O'Brien, R., J. E. Ladbury, and B. Z. Chowdry, in *Protein-Ligand Interactions: Hydrodynamics and Calorimetry*, edited by S. E. Harding and B. Z. Chowdry (Oxford University Press, New York, 2000), Chap. 10.

Oppong, F. K., P. Coussot, and J. R. de Bruyn, "Gelation on the microscopic scale," Phys. Rev. E **78**, 021405 (2008).

Oppong, F. K., and J. R. de Bruyn, "Diffusion of microscopic tracer particles in a yield-stress fluid," J. Non-Newtonian Fluid Mech. **142**, 104–111 (2007).

Oppong, F. K., L. Rubatat, B. J. Frisken, A. E. Bailey, and J. R. de Bruyn, "Microrheology and structure of a yield-stress polymer gel," Phys. Rev. E **73**, 041405 (2006).

Petit, L., C. Barentin, J. Colombani, C. Ybert, and L. Bocquet, "Size dependence of tracer diffusion in a Laponite colloidal gel," Langmuir **25**, 12048–12055 (2009).

Pignon, F., A. Magnin, J. M. Piau, B. Cabane, P. Lindner, and O. Diat, "Yield stress thixotropic clay suspension: Investigation of structure by light, neutron, and x-ray scattering," Phys. Rev. E **56**, 3281–3289 (1997).

Pignon, F., J.-M. Piau, and A. Magnin, "Structure and pertinent length scale of a discotic clay gel," Phys. Rev. Lett. **76**, 4857–4860 (1996).

Ramsay, J. D. F., "Colloidal properties of synthetic hectorite clay dispersions: I. Rheology," J. Colloid Interface Sci. **109**, 441–447 (1986).

Russel, W. B., D. A. Saville, and W. R. Schowalter, *Colloidal Dispersions* (Cambridge University Press, New York, 1989).

Ruzicka, B., L. Zulian, and G. Ruocco, "More on the phase diagram of Laponite," Langmuir **22**, 1106–1111 (2006).

Savin, T., and P. S. Doyle, "Role of a finite exposure time on measuring an elastic modulus using microrheology," Phys. Rev. E **71**, 041106 (2005a).

Savin, T., and P. S. Doyle, "Static and dynamic errors in particle tracking microrheology," Biophys. J. **88**, 623–638 (2005b).

Savin, T., and P. S. Doyle, "Electrostatically tuned rate of peptide self-assembly resolved by multiple particle tracking," Soft Matter **3**, 1194–1202 (2007a).

Savin, T., and P. S. Doyle, "Statistical and sampling issues when using multiple particle tracking," Phys. Rev. E **76**, 021501 (2007b).

Shalkevich, A., A. Stradner, S. K. Bhat, F. Muller, and P. Schurtenberger, "Cluster, glass, and gel formation and viscoelastic phase separation in aqueous clay suspensions," Langmuir **23**, 3570–3580 (2007).

Sollich, P., F. Lequeux, P. Hébraud, and M. E. Cates, "Rheology of soft glassy materials," Phys. Rev. Lett. **78**,

2020 (1997).

Squires, T. M., and T. G. Mason, "Fluid mechanics of microrheology," Annu. Rev. Fluid Mech. **42**, 413–438 (2010).

Strachan, D. R., G. C. Kalur, and S. R. Raghavan, "Size-dependent diffusion in an aging colloidal glass," Phys. Rev. E **73**, 041509 (2006).

Tawari, S. L., D. L. Koch, and C. Cohen, "Electrical double-layer effects on the Brownian diffusivity and aggregation rate of Laponite clay particles," J. Colloid Interface Sci. **240**, 54–66 (2001).

Thompson, D. W., and J. T. Butterworth, "The nature of Laponite and its aqueous dispersions," J. Colloid Interface Sci. **151**, 236–243 (1992).

Valentine, M. T., P. D. Kaplan, D. Thota, J. C. Crocker, T. Gisler, R. K. Prud'homme, M. Beck, and D. A. Weitz, "Investigating the microenvironments of inhomogeneous soft materials with multiple particle tracking," Phys. Rev. E **64**, 061506 (2001).

Valentine, M. T., Z. E. Perlman, M. L. Gardel, J. H. Shin, P. Matsudaira, T. J. Mitchison, and D. A. Weitz, "Colloid surface chemistry critically affects multiple particle tracking measurements of biomaterials," Biophys. J. **86**, 4004–4014 (2004).

van Megen, W., S. M. Underwood, and P. N. Pusey, "Nonergodicity parameters of colloidal glasses," Phys. Rev. Lett. **67**, 1586–1589 (1991).

van Olphen, H., *An Introduction to Clay Colloid Chemistry* (Wiley, New York, 1977).

Volkov, V. S., and A. I. Leonov, "Non-Markovian Brownian motion in a viscoelastic fluid," J. Chem. Phys. **104**, 5922–5931 (1996).

Waigh, T. A., "Microrheology of complex fluids," Rep. Prog. Phys. **68**, 685–742 (2005).

Weeks, E. R., J. C. Crocker, A. C. Levitt, A. Schofield, and D. A. Weitz, "Three-dimensional direct imaging of structural relaxation near the colloidal glass transition," Science **287**, 627–631 (2000).

Weeks, E. R., and D. A. Weitz, "Subdiffusion and the cage effect studied near the colloidal glass transition," Chem. Phys. **284**, 361–367 (2002).

Wegmann, M., B. Michen, T. Luxbacher, J. Fritsch, and T. Graule, "Modification of ceramic microfilters with colloidal zirconia to promote the adsorption of viruses from water," Water Res. **42**, 1726–1734 (2008).

Zaccarelli, E., "Colloidal gels: Equilibrium and non-equilibrium routes," J. Phys.: Condens. Matter **19**, 323101 (2007).